DOI: 10.1002/chem.200903355

Chiral Transformation in Protonated and Deprotonated Adipic Acids through Multistep Internal Proton Transfer

Seung Kyu Min,[a] Mina Park,[a] N. Jiten Singh,[a] Han Myoung Lee,[a] Eun Cheol Lee,[a] Kwang S. Kim,*[a] Anita Lagutschenkov,[b] and Gereon Niedner-Schatteburg*[c]

Abstract: Protonated and deprotonated adipic acids (PAA: $HOOC-(CH_2)_4-COOH_2^+$ and DAA: $HOOC-(CH_2)_4-COO^-$) have a charged hydrogen bond under the influence of steric constraint due to the molecular skeleton of a circular ring. Despite the similarity between PAA and DAA, it is surprising that the lowest energy structure of PAA is predicted to have $(H_2O\cdots H\cdots OH_2)^+$ Zundel-like symmetric hydrogen bonding, whereas that of DAA has H_3O^+ Eigen-like asymmetric hydrogen bonding. The energy profiles show that direct proton transfer between mirror image structures is unfavorable. Instead, the chiral transformation is possible by subsequent backbone twistings through stepwise proton transfer along multistep intermediate structures, which are Zundel-like ions for PAA and Eigen-like ions for DAA. This type of chiral transformation by multistep intramolecular proton transfers is unprecedented. Several prominent OH···O short hydrogen-bond stretching peaks are predicted in the range of 1000–1700 cm^{-1} in the Car–Parrinello molecular dynamics (CPMD) simulations, which show distinctive signatures different from ordinary hydrogen-bond peaks. The O–H–O stretching peaks in the range of 1800–2700 cm^{-1} become insignificant above around 150 K and are almost washed out at about 300 K.

Keywords: ab initio calculations · adipic acid · chirality · density functional calculations · proton transfer · vibrational spectroscopy

Introduction

The solvation of protonated molecular species has been a challenging subject of advanced spectroscopic studies for decades. Recent progress has arisen from the experimental[1] and theoretical[2,3] investigation of protonated water clusters. Charged hydrogen bonding prevails preferentially in either an Eigen or Zundel form.[4] Preferential localization of the extra proton at only one of the two acceptor sites indicates an asymmetric hydrogen bond. This situation is reminiscent of the Eigen cation H_3O^+.[5] Delocalization of a proton across a hydrogen bond occurs in a more symmetric situation, as in $H_5O_2^+$, known as Zundel cation.[6] The gradual transition between the two archetypes of ions was recently investigated as a function of relative basicity of the two proton acceptor sites, and a close relationship was revealed.[7] However, no studies have dealt with the influence of steric constraints for such charged hydrogen bonds so far.

The dicarboxylic acids provide two carboxo groups (acting as possible proton acceptor sites) that are linked by an alkylic chain. We chose the adipic acid that comprises chain length $n=4$ and studied its protonated form $C_6H_{11}O_4^+$ (PAA) and its deprotonated form $C_6H_9O_4^-$ (DAA). Hydrogen bonding between the two carboxylic acids yields cyclic forms that possess axial chirality along the hydrogen bond. Direct proton transfer amongst the two carboxylic residues is highly unfavorable. On the other hand, a chiral isomer of the cyclic protonated and deprotonated adipic acids can transform to another chiral isomer by virtue of twisting of the molecular skeleton, arising from the internal proton transfer between two terminal carboxylic acids that are

[a] S. K. Min, Dr. M. Park, Prof. N. J. Singh, Prof. H. M. Lee, Dr. E. C. Lee, Prof. Dr. K. S. Kim
Center for Superfunctional Materials, Department of Chemistry
Pohang University of Science and Technology, San 31
Hyojadong, Namgu, 790-784 Pohang (South Korea)
Fax: (+82) 54-279-8137
E-mail: kim@postech.ac.kr

[b] Dr. A. Lagutschenkov
Technische Universität Berlin, Institut für Optik und Atomare Physik
Hardenbergstraße 36, 10623 Berlin (Germany)

[c] Prof. Dr. G. Niedner-Schatteburg
Fachbereich Chemie and Forschungszentrum OPTIMAS
Technische Universität Kaiserslautern, Erwin-Schrödinger-Straße 52
67663 Kaiserslautern (Germany)
Fax: (+49) 631-205-2750
E-mail: gns@chemie.uni-kl.de

Supporting information for this article is available on the WWW under http://dx.doi.org/10.1002/chem.200903355.

equally stable. Most often, organic axial chiral isomers do not convert into each other. Their synthesis often requires completely different synthetic schemes. Unlike in the case of previously known axial chiral compounds in which the axis of chirality could be a single (as in atropisomers) or double bond (as in certain allene compounds), it is the O–H···O bond that represents the axis of chirality in the cyclic protonated and deprotonated adipic acids. It could be noted here that cyclic protonated and deprotonated adipic acids do not possess a stereogenic center to treat their topological isomers as enantiomers. In this context, it is of importance to investigate the chiral transformation in protonated and deprotonated adipic acids by internal proton transfer driven topological changes.

Computational Details

Low-lying isomers of PAA and DAA were initially located by optimizing more than 300000 initial configurations based on a density functional tight binding (DFTB)[8] annealing method.[9] These low-lying energy structures were reoptimized by using density functional theory and Møller–Plesset second order theory (MP2) with the aug-cc-pVDZ (aVDZ) basis set. Relative energies of the structures were studied with MP2 and coupled cluster theory with single, double, and perturbative triple excitations (CCSD(T)) at the complete basis set (CBS) limit.[10] Ab initio calculations were carried out by using the Gaussian suite of programs.[11] First principles CPMD simulations[12] of PAA and DAA were carried out for 10 ps at 150 and 300 K with the BLYP functional, a fictitious electron mass of 600 a.u. and an integration step of $\Delta t = 0.1$ fs. A Nosé–Hoover thermostat[13] ensured proper thermalization and we applied an isolated cubic box ($L = 13$ Å), a Poisson solver by the Tuckerman method on reciprocal,[14] and a norm-conserving Troulier–Martins pseudopotential.[15] Valence wave functions were expanded by plane waves with an energy cutoff value of 90 Ry. The potential hypersurface along the proton transfer was inspected by using the radial distribution functions (RDF) from CPMD simulations.

Results and Discussion

Structure calculations based on high-level ab initio theory reveal low-lying isomers **p1**–**p3** for PAA and **d1**–**d3** for DAA (Figure 1), all of which are cyclic through hydrogen bonding. Ring opening destabilizes these isomers by more than 50 kJ mol^{-1}.

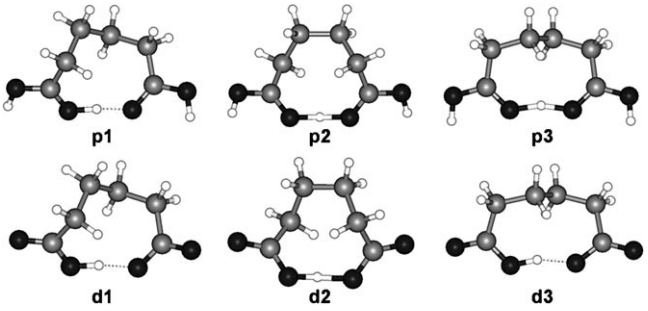

Figure 1. Structures of a) protonated adipic acid (PAA, isomers **p1**–**p3**) and b) deprotonated adipic acid (DAA, isomers **d1**–**d3**).

Through investigation of a one-dimensional view of the potential hypersurface along the proton transfer and by inspection of the radial distribution functions (RDF) from CPMD simulations[11] (Figure 2), we classify isomers **p1** and **d1** (and **d3**) as "Eigen-type" ions, and isomers **p2**, **p3**, and **d2** as "Zundel-type" ions (although **p3** and **d2** reveal some characteristics of the Eigen type). Isomer **d3** has somewhat higher energy with a longer hydrogen-bond than **d1** and **d2**, so we will not discuss it further because it has a clear Eigen-type hydrogen bond (r_{O1H}: 1.044 Å, r_{O2H}: 1.492 Å at the MP2/aVDZ level) (Table S1 in the Supporting Information). Isomer **d1** shows a noncentrosymmetric Eigen feature, whereas **d2** shows a partly centrosymmetric Zundel-like feature (though the Eigen-like feature is slightly retained). These features contrast that of the protonated water dimer ($H_5O_2^+$) for which the equilibrium r_{OO} is approximately 2.4 Å and the equilibrium r_{OH} is approximately 1.2 Å at the center of the r_{OO}, showing the centrosymmetric feature.[2c]

When comparing PAA and DAA, we note that the relative stability of **p3** with respect to **p1** is different from that of **d3** with respect to **d1**. For PAA, isomer **p3** is slightly

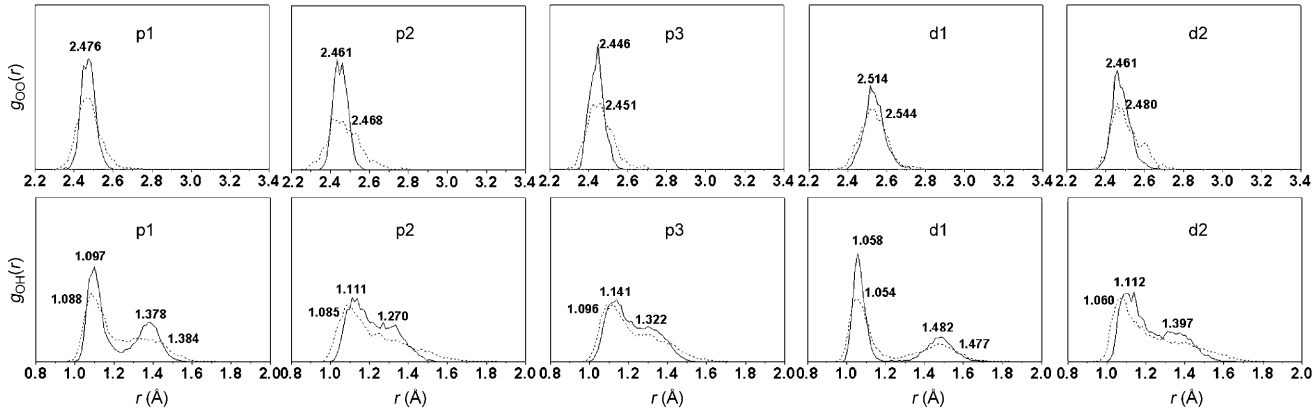

Figure 2. RDFs of g_{OO} and g_{OH} from the 150 (solid line) and 300 K (dashed line) CPMD simulations of protonated (**p1**, **p2**, **p3**) and deprotonated (**d1**, **d2**) adipic acids.

more stable than **p1**, whereas for DAA, isomer **d1** is much more stable than **d3**. Furthermore, the O–H–O stretching harmonic frequencies for **p3** appear around 1000–1100 cm^{-1}, whereas those of **d1** appear around 2200–2300 cm^{-1}. This should be correlated with the protonation energy at the specific O site depending on the H orientations. From a study on these local minima, we found that, in general, the proton was not on the midpoint of the O–H–O moiety, but tended to be bound to a specific O site in a single well-like potential instead of a double-well potential. As a specific example, we investigated the protonation energies of **d1**.

Separating the molecule into two fragments that contain four carbon atoms, we calculated the protonation energies for both fragments (Figure 3). The protonation energy for

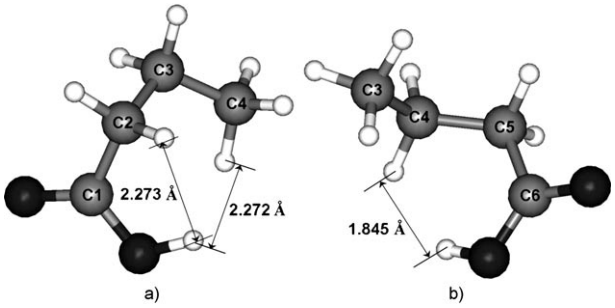

Figure 3. Structures of fragments **a** and **b** of **d1** for the protonation energy calculations. The protonation energy for **a** is 35.0 kJ mol^{-1} larger than that for **b** at the MP2/aVDZ level of theory mainly because of steric hindrance by a neighboring hydrogen atom near the attached proton. In **a**, the distance between H(C2) and the attached proton is 3.0 Å.

fragment **a** is 35.0 kJ mol^{-1} larger than that for fragment **b** at the MP2/aVDZ level. This difference would come partly from the steric hindrance between adjacent two hydrogen atoms as well as the skeletal orientation of the carbon chains. In the case of fragment **b**, the O–H and C4–C5 bonds are parallel and so the proton motion is hindered by the hydrogen at C4, whereas the O–H and C2–C3 bonds are perpendicular to each other, so the steric hindrance between two hydrogen atoms is minimized in the case of fragment **a**.

It is interesting to investigate possible pathways for internal proton transfer along the ionic hydrogen bond. A single-step direct proton transfer would need to switch the overall helical geometry at once. This would require a very high activation energy to break covalent bonds. Instead, a conceivable low-energy proton transfer proceeds through several sequential steps. Studying transition states between various conformers, we found that the optimal pathway of the proton transfer follows **p1**/**d1**→**T1**→**p2**/**d2**→**T2**→**p3**/**d3**→**T3**→$\overline{\textbf{p1}}$/$\overline{\textbf{d1}}$ (which is the mirror image of **p1**/**d1**) for PAA/DAA (Figures 4 and 5). Here, the transition state is denoted by **T**. From the initial conformation **p1**/**d1**, the C4 group rotates to form an eclipsed form with the C6 group at **T1**, and then the C4 group rotates further to form the **p2**/**d2** configuration. From the **p2**/**d2** conformation, the C4 group rotates

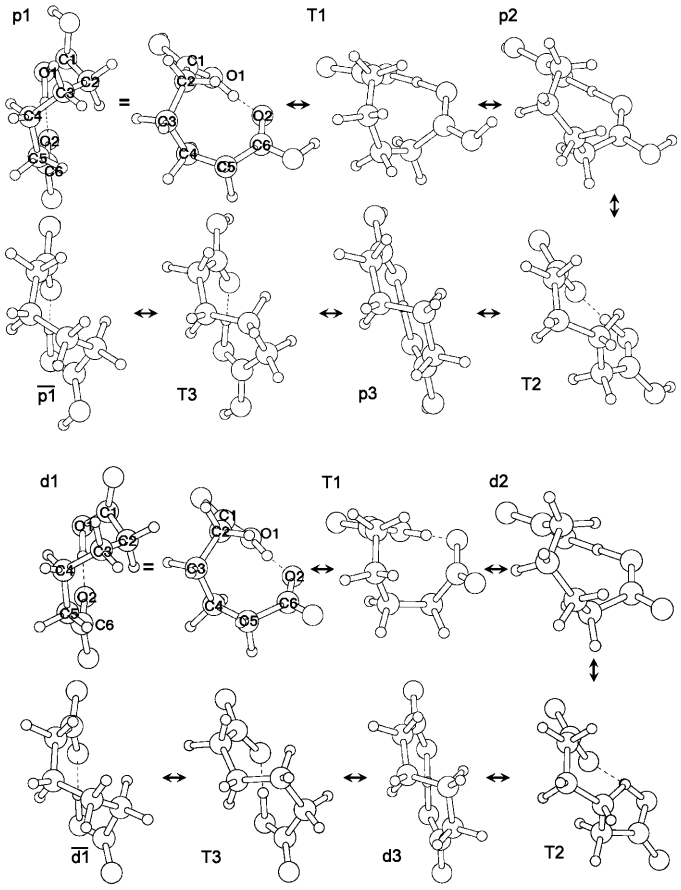

Figure 4. Isomerization pathway of PAA and DAA at the MP2/cVDZ level of theory. Top: $\overline{\textbf{p1}}$ is the mirror image of **p1.** **T1**, **T2**, and **T3** are transition states between two adjacent conformers. Three consecutive Hula-Hoop-like twists of the alkyl backbone enable proton transfer along the hydrogen bond between the two carboxo groups. Bottom: **d1** is the mirror image of **d1.** **T1**, **T2**, and **T3** are transition states between two adjacent conformers. As in the PAA case, proton transfer is directed by the angular isomerization of the alkyl chain.

so that the C3 and C4 groups eclipse each other at **T2**, and the C4 group keeps rotating in the same direction to form **p3**/**d3**. In this process, the helical direction of the carbon chain changes. Finally, the C4 and C5 groups rotate along the C4–C5 axis to form the $\overline{\textbf{p1}}$/$\overline{\textbf{d1}}$ conformation so that the proton is transferred and the helical direction is changed.

The conformational changes (ϕ versus θ maps) are plotted in terms of the dihedral angle (ϕ) of C2-C3-C4-C5 and the pseudo-dihedral angle (θ) between C2–C3 and O1–O2, which were obtained from the geometry optimization steps starting from more than 300 000 initial geometries generated at 1000–1500 K by the annealing method (Figure 5 and the Supporting Information). The energetics of these pathways were further optimized at the MP2/cVDZ level. Stepwise backbone twists enable proton transfer of **p1**→$\overline{\textbf{p1}}$ and **d1**→$\overline{\textbf{d1}}$ via a series of intermediate isomers. In a way, the Hula-Hoop-like twisting of the backbone acts as a switch that steers the location of the bound proton. The maximum transition barrier from **p1** to **p2** to **p3** to $\overline{\textbf{p1}}$ … to **p1** is less than 40 kJ mol^{-1}, and the maximum transition barrier from **d1** to

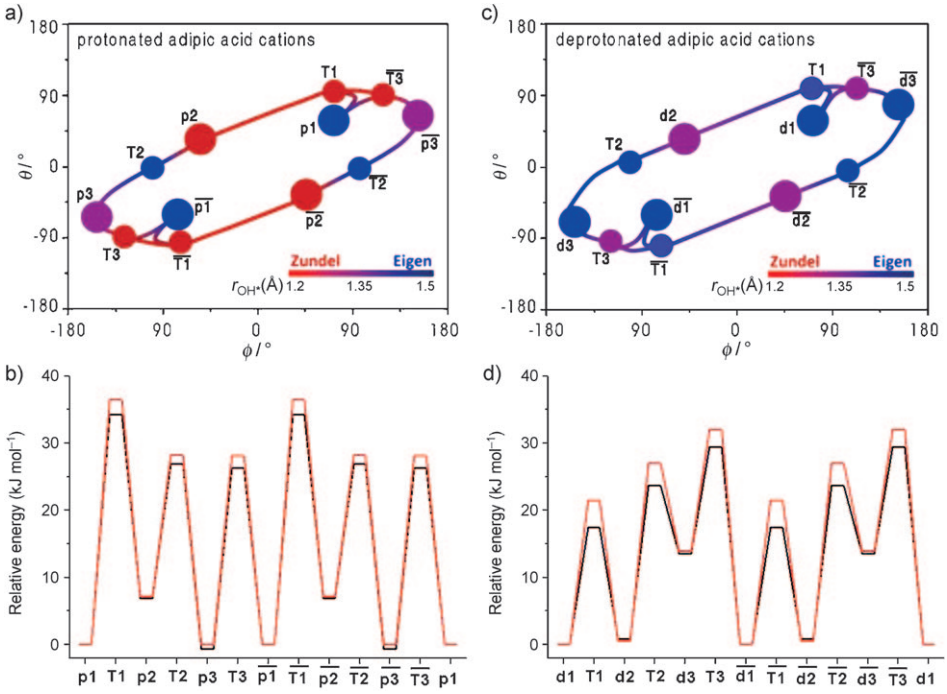

Figure 5. Conformational change (a) and energy profile (b; ΔE_0 in black; ΔG_{298K} in red) for the internal proton transfer pathways of PAA and those of DAA (c, d). The relative energies are calculated at the MP2/cVDZ level of theory. The conformational change is plotted from the DFTB geometry optimization steps starting with 300000 initial geometries generated by the annealing method. The conformational changes (ϕ versus θ maps) are plotted in terms of the dihedral angle (ϕ) of C2-C3-C4-C5 and the pseudo-dihedral angle (θ) between C2−C3 and O1−O2. The contour lines linking the stable and transition-state structures were drawn from the plot of all the trajectories starting from the 300000 initial geometries (see the Supporting Information). The energy profiles in (b, d) clearly reveal the multistep characters of the proton transfer. PAA shows some of Zundel-like structures (red colors) (except **T2**, $\overline{\mathbf{T2}}$) for the conformational changes in the outer ring (-**T1**-**p2**-**T2**-**P3**-**T3**-$\overline{\mathbf{T1}}$-**p2**-$\overline{\mathbf{T2}}$-**p3**-$\overline{\mathbf{T3}}$-$\overline{\mathbf{T1}}$-) in (a), but the Eigen-like structures inside the ring (blue colors) (**P1**, $\overline{\mathbf{P1}}$) in (a). This is because the cationic hydrogen bond has a very short bond length. DAA shows almost Eigen-like structures for the conformational changes in the outer ring as well as inside the ring (blue colors) in (c). This is because the anionic hydrogen bond has a slightly longer bond length than the cationic hydrogen bond.

d2 to **d3** to $\overline{\mathbf{d1}}$ … to **d1** is less than 35 kJ mol^{-1} (Figure 5). Though the transformation from one structure to another is not easy, it is still possible to obtain the equilibrium population within seconds. Thus, the spectra of these ions would reflect the relative stability of each conformer. In this regard, at room temperature we expect that **p3** would be the dominant species in PAA with some portion of **p1**, whereas **d1** would be the dominant species in DAA with a small fraction of **d2** (cf. Table 1).

The computed energy profiles clearly show that the direct proton transfer between **p1**↔$\overline{\mathbf{p1}}$ or between **p2**↔$\overline{\mathbf{p2}}$ is unfavorable. Instead, subsequent backbone twistings enable stepwise proton transfer along multistep intermediate structures, most of which are Zundel-like ions for PAA, but Eigen-like ions for DAA. It could imply interconversion of Eigen- and Zundel-type isomers in PAA and DAA. The charges of the O atoms (q_O) in the cationic hydrogen bond, compared with those in the anionic hydrogen bond, are much less negative (e.g., $q_O = -0.90/-0.90$ a.u. in $H_5O_2^+$, $q_O = -1.11/-1.25$ a.u. in $H_3O_2^-$); hence, there is much less repulsion between the two O atoms, resulting in shorter hydrogen-bond lengths. Thus, the repulsion between two O atoms sharing the H atom is much smaller in the cationic hydrogen bond (≈2.4 Å for the inter-oxygen distance) than in the anionic hydrogen bond (≈2.5 Å for the inter-oxygen distance). This is the reason why the transfer process in PAA is more of Zundel type and that in DAA is more of Eigen type. In both cases, a chiral isomer of either the cyclic protonated or of the deprotonated adipic acids transforms to another equally stable chiral isomer by internal proton transfer from one carboxylic residue to another carboxylic residue. Such a chiral transformation by virtue of the Hula-Hoop-like molecular skeleton twisting through multistep intramolecular proton transfers shows an intriguing novel phenomenon in stereochemistry.

By using first principles CPMD simulations based on density functional theory (DFT) with the Becke–Lee–

Table 1. Relative energies [kJ mol^{-1}] of PAA (**p1–3**) and DAA (**d1–3**) at the CCSD(T) and MP2 level of theory using the aug-cc-pVDZ (aVDZ) and CBS basis sets.[a]

Method	Structure	$\triangle E_e$ [kJ mol^{-1}]	$\triangle E_0$ [kJ mol^{-1}]	$\triangle G_r$ [kJ mol^{-1}]
CCSD(T)/aVDZ	**p1**	0.00	0.00	0.00
	p2	11.5	5.99	5.40
	p3	0.67	−2.05	−1.09
	d1	0.00	0.00	0.00
	d2	10.4	7.20	6.45
	d3	14.1	12.1	12.3
MP2/CBS	**p1**	0.00	0.00	0.00
	p3	−0.28	−3.00	−2.04
	d1	0.00	0.00	0.00
	d2	9.39	6.17	5.42
CCSD(T)/CBS	**p1**	0.00	0.00	0.00
	p3	−0.40	−3.13	−2.17
	d1	0.00	0.00	0.00
	d2	9.45	6.25	5.53

[a] $\triangle E_e/\triangle E_0$ is the zero-point-energy (ZPE)-uncorrected/corrected internal energy and $\triangle G_r$ is the free energy at room temperature and 1 atm. The CCSD(T)/aVDZ//MP2/aVDZ energies are very close to the MP2/aVDZ energies. For the CCSD(T)/aVDZ results, the ZPE and thermal energies are used with the MP2/aVDZ values. The MP2/CBS energies were obtained with the extrapolation scheme by using the MP2/aVDZ and MP2/aVTZ values and the fact that the electron correlation is proportional to N^{-3} for the aug-cc-pV*N*Z basis sets.[10] Then, the CCSD(T)/CBS energies are estimated by assuming that $E(\text{CCSD(T)/CBS}) \approx E(\text{MP2/CBS}) + [E(\text{CCSD(T)/aVDZ}) - E(\text{MP2/aVDZ})]$.[10]

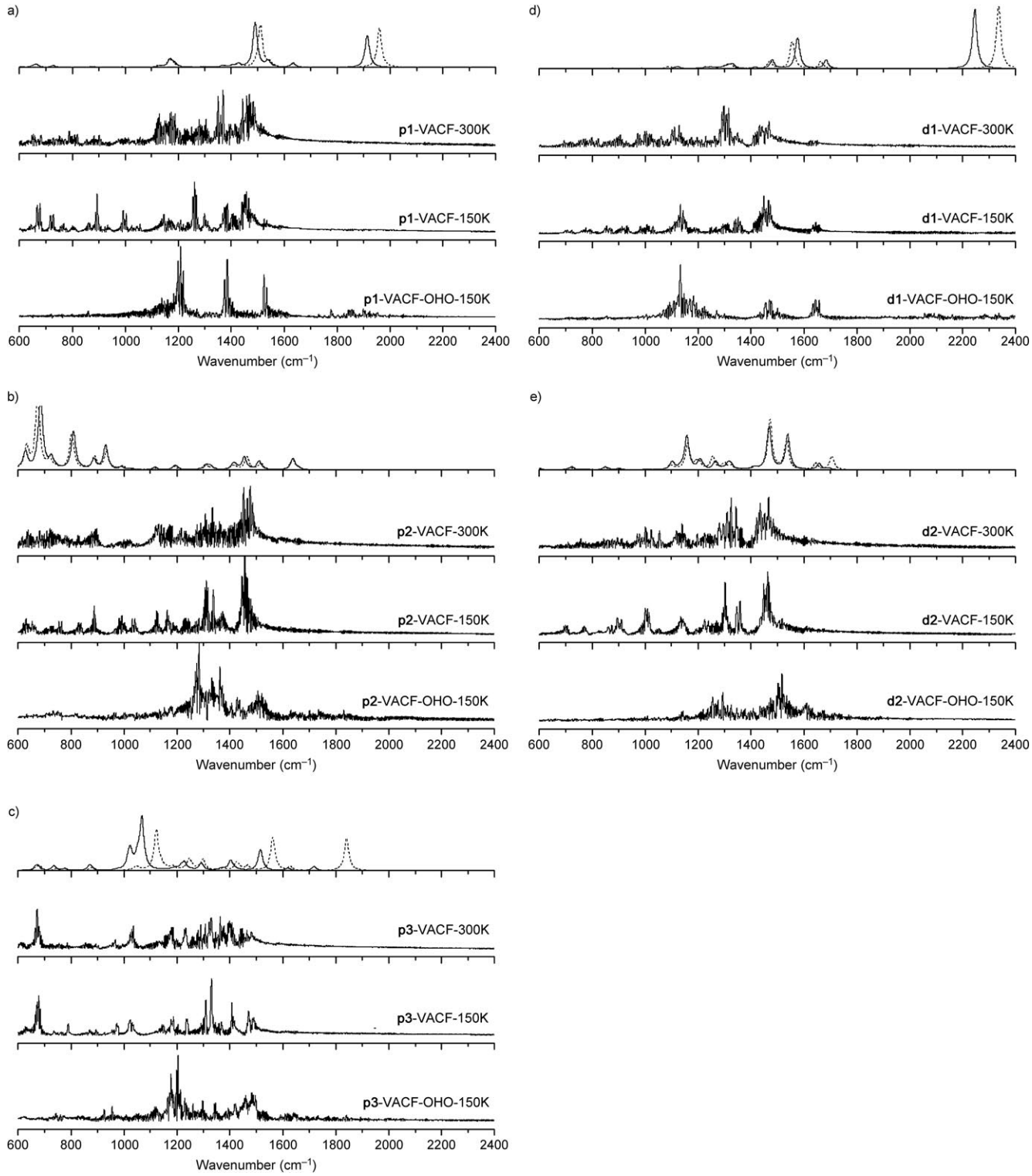

Figure 6. MP2/aVDZ (dotted lines) and B3LYP/aVDZ (black lines) scaled harmonic frequencies (in a Lorentzian distribution with a broadening factor of 10 cm^{-1}; scale factor: 0.957 and 0.963, respectively), CPMD(FT-VACF)/(150 and 300 K) spectra and spectrum analysis based on the O–H–O vibrational motion at 150 K (scale factor: 1.04) for both PAA (**p1** (a), **p2** (b), and **p3** (c)) and DAA (**d1** (d) and **d2** (e)) (see the Supporting Information).

Yang–Parr (BLYP) functionals, we investigated the dynamics of PAA and DAA on their highly complicated multidimensional potential hypersurfaces, which cannot properly be represented by analytical functions. In these first principles simulations, the anharmonicity of the potential surface is properly taken into account. Fourier-transformed velocity

autocorrelation function (FT-VACF) spectra resemble IR absorption spectra closely, except for some deviations in relative intensity between different modes. However, the mode analysis corresponding to each mode including the O···H···O stretching/bending mode can be done from the FT-VACF spectra. The power spectra from the Fourier transform of dipole-moment autocorrelation functions (FT-DACF) is provided in the Supporting Information. In contrast to the DAA structures, the PAA structures have the free OH frequencies because of the O–H in the carboxylic acid group. According to the spectral component analysis of the FT-VACF spectra,[2c] the frequencies of **p1**/**p3** (Figure 6) are assigned as $\nu_s = 1836/957$, $\nu_{bi} = 1388/1483$, and $\nu_{bo} = 1207/1204$, and $\nu_{CO} = 1592/1650\ cm^{-1}$. We note that the ν_s peaks in room-temperature CPMD simulations are smaller and more broadened than those in ab initio spectra. Even though **p1** can be substantially populated, as the temperature changes from 150 to 300 K, the ν_s peak of **p1** around $1800\ cm^{-1}$ would disappear due to the dynamic thermal broadening effect. This confirms that the spectra of short hydrogen bonds can be characterized only at very low temperatures, as discussed in previous works.[3] All isomers reveal no IR intensities beyond $1800\ cm^{-1}$ above 150 K.

The O–H···O stretching frequencies for PAA and DAA are in remarkable contrast to those of $H_5O_2^+$ and $H_3O_2^-$. Compared with the normal O–H···O bending frequency in the protonated water dimer ($\approx 1750\ cm^{-1}$),[1b] the corresponding bands in DAA and PAA (around $\approx 1500\ cm^{-1}$) are very weak. The calculated values of the O–H–O stretching modes in PAA and DAA ($\approx 1850/2200\ cm^{-1}$) point to a stiff potential that is highly restrained. The ring-shaped structure makes the vibration take place between hard walls composed of the molecular skeleton, resulting in higher stretching vibrational frequencies. This is in contrast with the protonated/deprotonated water dimer for which the proton vibration takes place between very soft walls since the O atoms can move almost freely without serious blocking by other neighboring atoms or molecular skeleton, resulting in lower vibrational frequencies.

Conclusion

For the case of PAA, two conformers (**p3** and **p1**) are particularly stable, while for DAA one conformer (**d1**) is particularly stable. We note from CPMD simulations that the O–H–O stretching frequencies around 1800–2700 cm^{-1} almost disappear due to the dynamic thermal broadening effect above 150 K.

The O atoms in O–H–O of the adipic acids experience steric constraints from the molecular skeleton, so that the H atom is highly bound to hard walls by a high barrier along the stretching mode. Thus, the O–H–O stretching frequency is high without showing the Zundel-like form. On the other hand, for the O–H–O mode of the protonated water dimer the H atom may be weakly bound to very soft walls in a very flat potential surface along the stretch mode and shows the Zundel-like low frequency. An activated proton transfer along the hydrogen bond would be feasible only along a high energy pathway that comprises a set of three Hula-Hoop backbone twists that interconvert otherwise well-separated conformers. This type of chiral transformations through multistep Zundel- and Eigen-like intramolecular proton transfers for PAA and DAA, respectively, is unprecedented and has not been predicted or observed before, showing an intriguing novel phenomenon in stereochemistry. Experiments on, for example, the IR spectroscopy of isolated cold PAA and DAA ions would be worthwhile to complement the present findings.

Acknowledgements

This work was supported by European Union N.E.S.T. (grant 015637), NRF (WCU: R32-2008-000-10180-0, EPB Center 2009-0063312, National Scientist Support Program, BK21, GRL), and KISTI (KSC-2008K08-0002).

[1] a) J. C. Jiang, Y. S. Wang, H. C. Chang, S. H. Lin, Y. T. Lee, G. Niedner-Schatteburg, H. C. Chang, *J. Am. Chem. Soc.* **2000**, *122*, 1398–1410; b) J. M. Headrick, E. G. Diken, R. S. Walters, N. I. Hammer, R. A. Christie, J. Cui, E. M. Myshakin, M. A. Duncan, M. A. Johnson, K. D. Jordan, *Science* **2005**, *308*, 1765–1769; c) M. Miyazaki, A. Fujii, T. Ebata, N. Mikami, *Science* **2004**, *304*, 1134–1137; d) J.-W. Shin, N. I. Hammer, E. G. Diken, M. A. Johnson, R. S. Walters, T. D. Jaeger, M. A. Duncan, R. A. Christie, K. D. Jordan, *Science* **2004**, *304*, 1137–1140; e) C.-C. Wu, C. K. Lin, H. C. Chang, J. C. Jiang, J. L. Kuo, M. L. Klein, *J. Chem. Phys.* **2005**, *122*, 074315–1–9; f) K. R. Asmis, N. L. Pivonka, G. Santambrogio, M. Brümmer, C. Kaposta, D. M. Neumark, L. Wöste, *Science* **2003**, *299*, 1375–1377; g) E. S. Stoyanov, I. V. Stoyanova, F. S. Tham, C. A. Reed, *J. Am. Chem. Soc.* **2008**, *130*, 12128–12138; h) E. S. Stoyanov, I. V. Stoyanova, C. A. Reed, *Chem. Eur. J.* **2008**, *14*, 3596–3604.

[2] a) O. Vendrell, F. Gatti, H. D. Meyer, *Angew. Chem.* **2007**, *119*, 7043–7046; *Angew. Chem. Int. Ed.* **2007**, *46*, 6918–6921; b) N. I. Hammer, E. G. Diken, J. R. Roscioli, E. M. Myshakin, K. D. Jordan, A. B. McCoy, X. Huang, S. Carter, J. M. Bowman, M. A. Johnson, *J. Chem. Phys.* **2005**, *122*, 244301; c) M. Park, I. Shin, N. J. Singh, K. S. Kim, *J. Phys. Chem. A* **2007**, *111*, 10692–10702; d) I. Shin, M. Park, S. K. Min, E. C. Lee, S. B. Suh, K. S. Kim, *J. Chem. Phys.* **2006**, *125*, 234305; e) D. Marx, M. E. Tuckerman, M. Parrinello, *J. Phys. Condens. Matter* **2000**, *12*, 153–159.

[3] N. J. Singh, M. Park, S. K. Min, S. B. Suh, K. S. Kim, *Angew. Chem.* **2006**, *118*, 3879–3884; *Angew. Chem. Int. Ed.* **2006**, *45*, 3795–3800.

[4] G. Niedner-Schatteburg, *Angew. Chem.* **2008**, *120*, 1024–1027; *Angew. Chem. Int. Ed.* **2008**, *47*, 1008–1011.

[5] M. Eigen, *Angew. Chem.* **1963**, *75*, 489–508; *Angew. Chem. Int. Ed. Engl.* **1964**, *3*, 1–19.

[6] G. Zundel, H. Metzger, *Z. Phys. Chem. (Muenchen Ger.)* **1968**, *58*, 222–245.

[7] J. R. Roscioli, L. R. McCunn, M. A. Johnson, *Science* **2007**, *316*, 249–254.

[8] a) T. Frauenheim, G. Seifert, M. Elstner, T. Niehaus, C. Köhler, M. Amkreutz, M. Sternberg, Z. Hajnal, A. D. Carlo, S. Suhai, *J. Phys. Condens. Matter* **2002**, *14*, 3049–3084.

[9] K. S. Kim, M. Dupuis, G. C. Lie, E. Clementi, *Chem. Phys. Lett.* **1986**, *131*, 451–465.

[10] a) T. Helgaker, W. Klopper, H. Koch, J. Noga, *J. Chem. Phys.* **1997**, *106*, 9639–9646; b) S. K. Min, E. C. Lee, H. M. Lee, D. Y. Kim, D. Kim, K. S. Kim, *J. Comput. Chem.* **2008**, *29*, 1208–1221; c) E. C. Lee, D. Kim, P. Jurečka, P. Tarakeshwar, P. Hobza, K. S. Kim, *J. Phys. Chem. A* **2007**, *111*, 3446–3457.

[11] Gaussian 03, Revision C.02, M. J. Frisch, G. W. Trucks, H. B. Schlegel, G. E. Scuseria, M. A. Robb, J. R. Cheeseman, J. A. Montgomery, Jr., T. Vreven, K. N. Kudin, J. C. Burant, J. M. Millam, S. S. Iyengar, J. Tomasi, V. Barone, B. Mennucci, M. Cossi, G. Scalmani, N. Rega, G. A. Petersson, H. Nakatsuji, M. Hada, M. Ehara, K. Toyota, R. Fukuda, J. Hasegawa, M. Ishida, T. Nakajima, Y. Honda, O. Kitao, H. Nakai, M. Klene, X. Li, J. E. Knox, H. P. Hratchian, J. B. Cross, C. Adamo, J. Jaramillo, R. Gomperts, R. E. Stratmann, O. Yazyev, A. J. Austin, R. Cammi, C. Pomelli, J. W. Ochterski, P. Y. Ayala, K. Morokuma, G. A. Voth, P. Salvador, J. J. Dannenberg, V. G. Zakrzewski, S. Dapprich, A. D. Daniels, M. C. Strain, O. Fartas, D. K. Malick, A. D. Rabuck, K. Raghavachari, J. B. Foresman, J. V. Ortiz, Q. Cui, A. G. Baboul, S. Clifford, J. Cioslowski, B. B. Stefanov, G. Liu, A. Liashenko, P. Piskorz, I. Komaromi, R. L. Martin, D. J. Fox, T. Keith, M. A. Al-Laham, C. Y. Peng, A. Nanayakkara, M. Challacombe, P. M. W. Gill, B. Johnson, W. Chen, M. W. Wong, C. Gonzalez, J. A. Pople, Gaussian, Inc., Pittsburgh PA, **2003**.

[12] CPMD code Version 3.7.2, CPMD, Copyright IBM Corp. 1990–2001, Copyright MPI für Festkörperforschung Stuttgart, **1997–2001**.

[13] a) S. Nose, *J. Chem. Phys.* **1984**, *81*, 511–519; b) W. G. Hoover, *Phys. Rev. A* **1985**, *31*, 1695–1697.

[14] G. J. Martyna, M. E. Tuckerman, *J. Chem. Phys.* **1999**, *110*, 2810–2821.

[15] a) N. Troullier, J. L. Martins, *Phys. Rev. B* **1991**, *43*, 1993–2006; b) M. Sprik, J. Hutter, M. Parrinello, *J. Chem. Phys.* **1996**, *105*, 1142–1152.

[16] W. S. Benedict, N. Gailar, E. K. Plyler, *J. Chem. Phys.* **1956**, *24*, 1139–1165.

Received: December 8, 2009
Revised: April 1, 2010
Published online: July 22, 2010

